Time evolution of wave packets on nanostructures

2005 J. Phys. A: Math. Gen. 38 4843

(http://iopscience.iop.org/0305-4470/38/22/009)

INSTITUTE OF PHYSICS PUBLISHING JOURNAL OF PHYSICS A: MATHEMATICAL AND GENERAL

J. Phys. A: Math. Gen. **38** (2005) 4843–4858 doi:10.1088/0305-4470/38/22/009

Time evolution of wave packets on nanostructures

E de Prunelé

Laboratoire de Physique Moléculaire, UMR CNRS 6624, Université de Franche Comté, 16 route de Gray, La Bouloie, 25030 Besançon Cedex, France

Received 19 July 2004, in final form 18 November 2004
Published 18 May 2005
Online at stacks.iop.org/JPhysA/38/4843

Abstract

Time evolution of wave packets on nanostructures is studied on the basis of a three-dimensional solvable model with singular interactions (de Prunelé 1997 *J. Phys. A: Math. Gen.* **30** 7831). In particular, methods and tools are provided to determine time independent upper bounds for the overlap of the normalized time-dependent wave packet with the time independent normalized wave packet concentrated at an arbitrarily chosen vertex of the nanosystem. The set of upper bounds referring to all initial positions of the wave packet and all overlaps are summarized in a matrix. The analytical formulation allows a detailed study for arbitrary geometrical configurations. Time evolution on truncated quasicrystalline systems has been found to be site selective, depending on the position of the initial wave packet.

PACS numbers: 02.30.−f, 03.65.Ge, 61.44.Br, 05.60.Gg

1. Introduction

Time evolution of a wave packet on a nanostructure is one aspect of the complex general transport problem. For general overviews of transport problems, see e.g. [1, 2]. For some recent work on wave packet time evolution, see e.g. [3–16]. References [4, 13, 14] are mainly concerned with the revival of wave packets, [5, 8–10] with the time evolution of wave packets in quasiperiodic or chaotic systems, [6, 7, 11, 12] with transport and tunelling phenomena. Finally, [16] is concerned with wave packets in atomic systems, namely Rydberg atoms. This paper is concerned with only one aspect of the general transport problem, the time evolution of a wave packet according to the Schrödinger equation

$$\mathrm{i}\hbar \frac{\mathrm{d}|\psi\rangle}{\mathrm{d}t} = H|\psi\rangle \tag{1}$$

within the independent particle framework. Here $|\psi\rangle$ is a one-particle state in three-dimensional space, and H is a time independent solvable Hamiltonian with singular interactions described in the next section.

Although conceptually simple, this problem is practically difficult to solve in the sense that it generally requires heavy numerical calculations. One is faced with a partial differential

equation involving four variables, one for time, three for space. For an arbitrary geometric configuration of the system described by the Hamiltonian H, there is no symmetry which allows us to simplify the calculations, for example by separation of the variables. Therefore solvable models are particularly helpful, especially for the study of the influence of the geometry of the system and of initial conditions. The presently used model, which will be described in section 2, solved in sections 3 and 4 and applied in section 5, demonstrates the importance of the geometry for time evolution and clearly shows that non-intuitive interesting effects are governed by the geometry only. In particular, the initial position of the wave packet plays a crucial role for subsequent time evolution in quasiperiodic systems. We stress that the geometric configuration of the system in three-dimensional space can be chosen at will in the present model.

2. The Hamiltonian

The presently used model is the simplest case of a more general solvable model described in detail in [17] and is therefore only briefly presented here with essentially the same notation as in [17]. The Hamiltonian is

$$H = \frac{p^2}{2m} + \sum_{j=1}^{N} V_j. \tag{2}$$

Atomic units (au) will be used. In configuration space, the operator p^2 acts as minus the three-dimensional Laplacian, $-\frac{\partial^2}{\partial x^2} - \frac{\partial^2}{\partial y^2} - \frac{\partial^2}{\partial z^2}$. The effective interaction at the centre characterized by the vector position $\mathbf{a}_j$ is a separable one:

$$V_j = \lambda |\xi_j\rangle\langle\xi_j| \tag{3}$$

$$|\xi_j\rangle = \exp(-\mathrm{i}\mathbf{a}_j \cdot \mathbf{p}) r^{3/2} |r, 0, 0\rangle \tag{4}$$

with $|r, 0, 0\rangle \equiv |r, \ell = 0, m = 0\rangle$ an eigenvector of the squared orbital angular momentum with eigenvalue $\ell(\ell + 1)$ an eigenvector of the component L_z of the orbital angular momentum with eigenvalue m (not to be confused with the mass in the kinetic energy term), and a generalized eigenvector of the radial position operator with a generalized eigenvalue r, normalized according to

$$\langle r', 0, 0 | r, 0, 0\rangle = \frac{\delta(r' - r)}{r^2} \qquad \langle \mathbf{r}' | r, 0, 0\rangle = \frac{\delta(r' - r)}{r^2} \frac{1}{\sqrt{4\pi}}. \tag{5}$$

All the eigenvalues are relative to an arbitrary fixed frame. The momentum operator is denoted by $\mathbf{p}$. The exponential term in equation (4) corresponds to a translation by a vector displacement $\mathbf{a}_j$. The lower index (presently j) corresponds to the position of the centre of the interaction V_j. The set of centre positions $\{\mathbf{a}_j\}$, $j = 1, \ldots, N$, is given, and will be referred to as a given geometric configuration of the system. The symbol d_{jk} will be used to denote the distance between centres j and k:

$$d_{jk} \equiv |\mathbf{a}_j - \mathbf{a}_k|.$$

The one-centre interaction (3) is thus a projector on the s partial wave relative to this centre. This interaction depends on two parameters only, λ, r. The strength of the interaction is characterized by λ, its range by r. For the case of *an isolated centre*, a bound state exists if $\lambda < -1/(2mr^2)$.

The free resolvent $G_0(z)$ is defined by

$$G_0(z) = \frac{1}{z - \frac{p^2}{2m}}$$

3. Eigenvalues and eigenvectors of the Hamiltonian

From now on z will denote a negative real variable (and therefore $G_0^\dagger(z) = G_0(z)$), and the purely imaginary number p with positive imaginary part will be related to z by $z = \frac{p^2}{2m}$.

The exact eigenvalues of H are the zeros of the determinant of a matrix b of order N with respect to the variable z:

$$b_{ij}(z) = \delta_{ij} - \lambda(g_0(z))_{ij} \tag{6}$$

$$(g_0(z))_{ij} \equiv \langle \xi_i | G_0(z) | \xi_j \rangle. \tag{7}$$

The explicit expressions for the matrix elements of G_0 are

$$\mathrm{if}\ d_{ji} \geqslant 2r, \qquad (g_0(z))_{ij} = -2mr^3 p \left(\frac{\sin(pr)}{pr}\right)^2 \left(\frac{\exp(\mathrm{i}pd_{ji})}{pd_{ji}}\right) \tag{8}$$

$$\mathrm{if}\ d_{ji} \leqslant 2r, \qquad (g_0(z))_{ij} = \frac{mr}{d_{ji}p^2}[\mathrm{i}\exp(\mathrm{i}p2r)\sin(pd_{ji}) - \exp(\mathrm{i}pd_{ji}) + 1]. \tag{9}$$

Equation (8) was derived in [17] and equation (9) can be obtained in a similar way by contour integration in the complex plane and use of the residue theorem. It can be verified that the two expressions coincide for $d_{ji} = 2r$, and that, in the limit $d_{ji} \to 0$, equation (9) gives the following expression for the diagonal matrix elements already obtained by direct integration [17]:

$$(g_0(z))_{jj} = -2mr^3 p \left(\frac{\exp(\mathrm{i}pr)}{pr}\right)\left(\frac{\sin(pr)}{pr}\right). \tag{10}$$

The exact normalized eigenvector of H corresponding to the eigenvalue z_u is

$$|\psi_u\rangle = \frac{G_0(z_u)\sum_i |\xi_i\rangle\langle\xi_i|\psi_u\rangle}{\sqrt{\sum_{j,k}\langle\psi_u|\xi_j\rangle\langle\xi_j|G_0^2(z_u)|\xi_k\rangle\langle\xi_k|\psi_u\rangle}}. \tag{11}$$

The coefficients $\langle\xi_i|\psi_u\rangle$ appearing in the numerator and denominator are the elements of a column eigenvector associated with the zero eigenvalue of the matrix $b\,(z_u)$. This matrix is real symmetric (for $z < 0$), and therefore the $\langle\xi_i|\psi_u\rangle$ can all be chosen real, this choice being made from now on.

The denominator of equation (11) can finally be computed from the following general results which will be needed in section 4:

$$\mathrm{if}\ d_{jk} \geqslant 2r, \qquad \langle\xi_j|G_0(z_2)G_0\,(z_1)\,|\xi_k\rangle = \frac{(2m)^2 r}{d_{jk}(p_2+p_1)}\frac{1}{(p_2-p_1)} \times\left[\frac{\sin^2(p_2 r)\exp(\mathrm{i}d_{jk}p_2)}{p_2^2} - \frac{\sin^2(p_1 r)\exp(\mathrm{i}d_{jk}p_1)}{p_1^2}\right] \tag{12}$$

$$\mathrm{if}\ d_{jk} \leqslant 2r, \qquad \langle\xi_j|G_0(z_2)G_0(z_1)|\xi_k\rangle = 2m^2\frac{r}{d_{jk}}\left\{\frac{1}{p_2^2 p_1^2} + \frac{1}{(p_2+p_1)(p_2-p_1)} \times\left[\begin{array}{c} -\mathrm{i}\exp(\mathrm{i}p_2 2r)\dfrac{\sin(p_2 d_{jk})}{p_2^2} + \mathrm{i}\exp(\mathrm{i}p_1 2r)\dfrac{\sin(p_1 d_{jk})}{p_1^2} \\ +\dfrac{\exp(\mathrm{i}p_2 d_{jk})}{p_2^2} - \dfrac{\exp(\mathrm{i}p_1 d_{jk})}{p_1^2} \end{array}\right]\right\}. \tag{13}$$

These results have been obtained by contour integration in the complex plane and the method is briefly outlined in the appendix. It can be verified that the two expressions coincide for $d_{ji} = 2r$, and that, in the limit $d_{ji} \to 0$, equation (13) gives the following expression for the diagonal matrix elements:

$$\langle \xi_j | G_0(z_2) G_0(z_1) | \xi_j \rangle = -\mathrm{i} \frac{2m^2 r}{p_1 + p_2} \left\{ \frac{1}{p_1 p_2} + \frac{1}{p_2 - p_1} \left[\frac{\exp(\mathrm{i}2p_2 r)}{p_2} - \frac{\exp(\mathrm{i}2p_1 r)}{p_1} \right] \right\}. \quad (14)$$

The denominator of equation (11) involves $\langle \xi_j | G_0^2(z_u) | \xi_k \rangle$ and therefore the limit $z_2 \to z_1$ in equations (12)–(14) has to be calculated. This limit corresponds essentially to derivation operations for the right-hand sides, and one obtains

$$\mathrm{if}\ d_{jk} \geqslant 2r, \qquad \langle \xi_j | G_0^2(z) | \xi_k \rangle = 2m^2 \frac{r}{d_{jk}} \frac{1}{p^4} \times \exp(\mathrm{i}pd_{jk}) \sin(pr)[\sin(pr)(\mathrm{i}d_{jk}p - 2) + 2pr\cos(pr)] \quad (15)$$

$$\mathrm{if}\ d_{jk} \leqslant 2r, \qquad \langle \xi_j | G_0^2(z) | \xi_k \rangle = 2m^2 \frac{r}{d_{jk}} \frac{1}{p^4} \left\{ 1 + \frac{1}{2} [\exp(\mathrm{i}p2r)((2\mathrm{i} + 2pr)\sin(pd_{jk}) - \mathrm{i}pd_{jk}\cos(pd_{jk})) + (-2 + \mathrm{i}pd_{jk})\exp(\mathrm{i}pd_{jk})] \right\} \quad (16)$$

$$\langle \xi_j | G_0^2(z) | \xi_j \rangle = \frac{2(mr)^2}{p^2} \exp(\mathrm{i}pr) \left[\exp(\mathrm{i}pr) - \frac{\sin(pr)}{pr} \right]. \quad (17)$$

Equations (15) and (17) correspond to equation (7) of [18] where they were obtained directly by contour integration. The wavefunction in configuration space can then be obtained from the explicit expression for $\langle \mathbf{r} | G_0(z) | \xi_i \rangle$ (see the equation below equation (7) of [18]),

$$\langle \mathbf{r} | G_0(z) | \xi_i \rangle = -\frac{mr^{3/2} p}{\sqrt{\pi}} \frac{\exp(\mathrm{i}pr_>)}{pr_>} \frac{\sin(pr_<)}{pr_<} \quad (18)$$

with $r_>, r_<$ the largest and smallest values respectively, of the range r of the interaction and the distance $|\mathbf{r} - \mathbf{a}_i|$ between the point where the wavefunction is computed and the centre $\mathbf{a}_i$.

Degeneracy may occur if the group of symmetry of the geometrical configuration has an irreducible representation of dimension greater than unity. The orthonormality relations

$$\langle \psi_u | \psi_v \rangle = \delta_{uv} \quad (19)$$

are automatically verified provided $z_u \neq z_v$, because eigenvectors of a Hermitian operator associated with different eigenvalues are orthogonal. In the case of degeneracy, $z_u = z_v$, it is assumed that orthogonalization has been achieved explicitly.

It has been shown [21] that the Hamiltonian H has at most N bound states $|\psi_u\rangle$. We stress that the only numerical part for the determination of the eigenvalues is the computation of the zeros of a determinant of a matrix of order N whose matrix elements are simple analytic functions. Then the only numerical part for the determination of the eigenvectors and their associated wavefunctions is the resolution of a system of linear equations of order N at most.

4. Transport along the system

4.1. The initial state

For the construction of the initial state (at the beginning of the transport phenomenon), we choose a state localized in the vicinity of a point $\mathbf{a}_d$, more specifically the normalized eigenstate of the *one-centre* Hamiltonian $h = \frac{p^2}{2m} + V_d$:

$$|\chi_d\rangle = \frac{G_0(z_0)|\xi_d\rangle}{\sqrt{\langle\xi_d|G_0^2(z_0)|\xi_d\rangle}}, \tag{20}$$

where z_0 is the negative eigenvalue of h. The position $\mathbf{a}_d$ can be arbitrary, but will be chosen to coincide with one of the centres of the nanosystem in the applications (see section 5). Thus when the index d is an integer between 1 and N, the position $\mathbf{a}_d$ coincides with a centre $\mathbf{a}_j$ ($1 \leqslant j \leqslant N$) of the nanosystem. We stress that the Hamiltonian (2) is a one-particle Hamiltonian *in three-dimensional space*, with arbitrary geometry for the centres $\mathbf{a}_j$. An arbitrary wave packet thus will not generally stay confined in the vicinity of the system but part of it will escape to infinity. To ensure confinement within the system, we project the state $|\chi_d\rangle$ onto the subspace of negative eigenvalues of the Hamiltonian H of the total system. Our initial state $|\varphi_d\rangle$ ($t = 0$) is thus $P|\chi_d\rangle/\langle\chi_d|P|\chi_d\rangle$, with P the projector onto the subspace. The solution for the time-dependent state is now described in detail.

4.2. Exact solution of the time-dependent Schrödinger equation

The projector P onto the eigensubspace of bound states is

$$P = \sum_{u=1}^{N_b} |\psi_u\rangle\langle\psi_u| \tag{21}$$

with the orthonormal eigenstates $|\psi_u\rangle$ of the Hamiltonian H given by equation (11). In equation (21), the index of summation runs over N_b ($\leqslant N$) values, the number of bound states of H. The projector P is Hermitian:

$$P = P^\dagger = P^2.$$

$P|\chi_d\rangle$ denotes the projection of the normalized one-centre state $|\chi_d\rangle$ onto the subspace of bound states of the total Hamiltonian H, and the initial state $|\varphi_d\rangle$ is $P|\chi_d\rangle$ normalized to unity:

$$\|P|\chi_d\rangle\|^2 = \langle\chi_d|P|\chi_d\rangle = \sum_{u=1}^{N_b} |\langle\psi_u|\chi_d\rangle|^2 \leqslant 1 \qquad |\varphi_d\rangle = \frac{P|\chi_d\rangle}{\sqrt{\langle\chi_d|P|\chi_d\rangle}}.$$

The inequality in the line above is the Bessel inequality. The computation of $P|\chi_d\rangle$ can be achieved from knowledge of the $\langle\psi_u|\chi_d\rangle$ which requires knowledge of $\langle\xi_i|G_0(z_u)G_0(z_0)|\xi_d\rangle$. These matrix elements can be obtained from equations (12), (13).

The time-dependent normalized state is then given by

$$\begin{aligned} |\varphi_d(t)\rangle &= \exp(-\mathrm{i}Ht)|\varphi_d\rangle \\ &= \frac{\sum_{u=1}^{N_b} \exp(-\mathrm{i}z_u t)|\psi_u\rangle\langle\psi_u|\chi_d\rangle}{\sqrt{\langle\chi_d|P|\chi_d\rangle}} \end{aligned} \tag{22}$$

and its wavefunction then follows from equation (18). It is clear from equation (22) that time evolution requires accurate determination of the eigenenergies z_u, especially when the difference between neighbouring energies is small, a characteristic feature of quasicrystalline systems.

It can be noted that equations (11)–(13) can be used to test the numerical accuracy of the computed matrix elements by testing the orthonormality relations (19).

Clearly $\langle\varphi_k(t)|\varphi_k(t)\rangle = 1$ since each $|\varphi_k(t)\rangle$ is normalized by the definition for $t = 0$ and remains normalized for all times t since H is Hermitian. The Schwarz inequality then yields $|\langle\varphi_j(t)|\varphi_k(t)\rangle| \leqslant 1$. For $j \neq k$, $\langle\varphi_j(t)|\varphi_k(t)\rangle$ is also time independent but is not equal to zero. Nevertheless, as $|\varphi_k(0)\rangle$ is localized in the vicinity of the centre $\mathbf{a}_k$, the overlap $\langle\varphi_j(t)|\varphi_k(t)\rangle$ decreases exponentially as the distance d_{jk} increases. Let us now introduce a matrix Φ of order N whose matrix elements are defined by

$$\Phi_{jk} = \langle\varphi_j(0)|\varphi_k(0)\rangle \tag{23}$$

$$= \langle\varphi_j(t)|\varphi_k(t)\rangle. \tag{24}$$

This matrix has unity on the main diagonal, and the Schwarz inequality ensures $|\Phi_{jk}| \leqslant 1$. Let us define the ratio R by

$$R = \frac{\sum_{j,k} |\Phi_{jk}|^2}{N}. \tag{25}$$

If $R \simeq 1$, and if $N_b = N$, the vectors $|\varphi_k(t)\rangle$ $(k = 1, \ldots, N)$ provide, for each time t, an approximate orthonormal basis for the subspace of bound states. Whether the ratio R is close to unity or not, the subsequent analysis remains valid.

A very convenient tool for visualizing wave packet time evolution, especially for long times and a complex geometry in three-dimensional space, is to plot for each centre j the square modulus matrix elements

$$P_{j,d}(t) \equiv |\langle\varphi_j(0)|\varphi_d(t)\rangle|^2 = \left| \frac{\sum_{u=1}^{N_b} \exp(-\mathrm{i}z_u t)\langle\chi_j|\psi_u\rangle\langle\psi_u|\chi_d\rangle}{\sqrt{\langle\chi_j|P|\chi_j\rangle\langle\chi_d|P|\chi_d\rangle}} \right|^2. \tag{26}$$

The left-hand side clearly is, for each time t, a measure of the overlap of the time-dependent wave packet $|\varphi_d(t)\rangle$ with a fictitious wave packet $|\varphi_j(0)\rangle$ which would be an initial wave packet centred at the centre j at time t. If $R \simeq 1$, this measure can be interpreted, loosely speaking, as the probability that the time-dependent state $|\varphi_d(t)\rangle$ is to be found near the centre $\mathbf{a}_j$, and $\sum_{j=1}^{N} P_{j,d}(t) \simeq 1$. If R is significantly greater than unity, the measures $P_{j,d}(t)$ are not normalized. The right-hand side of equation (26) can be computed very rapidly according to the previous results.

As the modulus of a sum is smaller than or equal to the sum of moduli, one has

$$P_{j,d}(t) \leqslant \frac{1}{\langle\chi_j|P|\chi_j\rangle\langle\chi_d|P|\chi_d\rangle} \left[\sum_{u=1}^{N_b} |\langle\chi_j|\psi_u\rangle\langle\psi_u|\chi_d\rangle| \right]^2 \equiv M_{j,d}. \tag{27}$$

The upper bounds $M_{j,d}$ are time independent, satisfy $M_{j,d} = M_{d,j}$ and will provide an extremely useful tool for subsequent analysis of time evolution on quasicrystalline systems. The matrix M will be called the majorant matrix. The Schwarz inequality $\sum_u a_u b_u \leqslant \sqrt{\sum_u |a_u|^2}\sqrt{\sum_u |b_u|^2}$ ensures that $M_{j,d} \leqslant 1$, and of course $M_{j,j} = 1$.

5. Some applications

From now on, the values of the strength parameter λ and of the range parameter r are $\lambda = -0.398\,909$ au and $r = 1.817\,6943$ au. These values are not critical, but this choice corresponds to the choices previously made [18–20] and was originally motivated for reproducing the band structure of lithium [19]. Moreover, in the applications presented below, the parameters r, λ and the geometric configuration parameters $\mathbf{a}_j$ are such that the system has indeed a maximum number of bound states, $N_b = N$.

5.1. Truncated periodic linear chain

As in [19], we take the common intercentre distance $d = d_{jk} = 6.5183\frac{\sqrt{3}}{2} \simeq 5.645$ au. The number of centres is $N = 14$. The time evolution of the modulus of the wavefunction on the chain axis is reported in figure 1. We take the departure index $d = 1$. This corresponds to a wave packet initially centred on the left extremity of the chain at time $t = 0$. The maximum time, $t = 431$ au, corresponds to a maximum value of the modulus of the wavefunction on the right extremity of the chain. This interval of time is subdivided into ten equidistant points ($t = k\,431/9$, $k = 0, 1, \ldots, 9$). One sees in figure 1 a regular evolution from left to right with a final concentration on the right extremity.

As $R \simeq 1.03$, (see equation (25)), the vectors $|\varphi_j(0)\rangle (j = 1, \ldots, N)$ provide an approximate orthonormal basis for the subspace of bound states, and $\sum_{j=1}^{N} P_{j,d}(t)$ is close to unity.

In order to better appreciate the time evolution in a continuous way, figure 2 reports the modulus of the overlap coefficients, $P_{j,1}(t)$ (see equation (26)) over the same time interval. The first overlap $P_{1,1}(t)$ (the thinner curve) begins by decreasing with time, and for $j \neq 1$ (other curves) each $P_{j,1}(t)$ first increases with time t, in the order of increasing j values. In figure 2, the sum $\sum_{j=1}^{14} P_{j,1}(t)$, slightly above unity, has small oscillations that remain invisible at the scale of the graph.

Figure 3 reports the overlap coefficient $P_{1,1}(t)$, equation (26), for a longer time interval ($t = 3000$), together with the sum of all $P_{j,1}(t)$ (thick dashed line). The local maxima of $P_{1,1}(t)$ nicely illustrate what has been called quantum wave packet revival, a phenomenon that occurs in many contexts [15, 16]. None of the curves is periodic with respect to time t. It is recalled that the wave packet must remain in the vicinity of the chain because we consider bound states in this paper. In the theory of revival phenomena, one typically expands the energy eigenvalues (supposed here to depend on one quantum number only), in a Taylor series around a mean energy level, see e.g. [13, 15]. The quadratic term leads to what has been called perfect revivals. It is emphasized that throughout the present work, the quantum revivals are not perfect because the spectrum is not quadratic in the quantum number. Finally, the majorant matrix M is

$$
\begin{array}{cccccccccccccc}
1.0 & 0.7 & 0.6 & 0.7 & 0.6 & 0.6 & 0.7 & 0.7 & 0.6 & 0.6 & 0.7 & 0.6 & 0.7 & 1.0 \\
0.7 & 1.0 & 0.6 & 0.7 & 0.6 & 0.6 & 0.7 & 0.7 & 0.6 & 0.6 & 0.7 & 0.6 & 1.0 & 0.7 \\
0.6 & 0.6 & 1.0 & 0.6 & 0.5 & 0.8 & 0.6 & 0.6 & 0.8 & 0.5 & 0.6 & 1.0 & 0.6 & 0.6 \\
0.7 & 0.7 & 0.6 & 1.0 & 0.6 & 0.6 & 0.7 & 0.7 & 0.6 & 0.6 & 1.0 & 0.6 & 0.7 & 0.7 \\
0.6 & 0.6 & 0.5 & 0.6 & 1.0 & 0.5 & 0.6 & 0.6 & 0.5 & 1.0 & 0.6 & 0.5 & 0.6 & 0.6 \\
0.6 & 0.6 & 0.8 & 0.6 & 0.5 & 1.0 & 0.6 & 0.6 & 1.0 & 0.5 & 0.6 & 0.8 & 0.6 & 0.6 \\
0.7 & 0.7 & 0.6 & 0.7 & 0.6 & 0.6 & 1.0 & 1.0 & 0.6 & 0.6 & 0.7 & 0.6 & 0.7 & 0.7 \\
0.7 & 0.7 & 0.6 & 0.7 & 0.6 & 0.6 & 1.0 & 1.0 & 0.6 & 0.6 & 0.7 & 0.6 & 0.7 & 0.7 \\
0.6 & 0.6 & 0.8 & 0.6 & 0.5 & 1.0 & 0.6 & 0.6 & 1.0 & 0.5 & 0.6 & 0.8 & 0.6 & 0.6 \\
0.6 & 0.6 & 0.5 & 0.6 & 1.0 & 0.5 & 0.6 & 0.6 & 0.5 & 1.0 & 0.6 & 0.5 & 0.6 & 0.6 \\
0.7 & 0.7 & 0.6 & 1.0 & 0.6 & 0.6 & 0.7 & 0.7 & 0.6 & 0.6 & 1.0 & 0.6 & 0.7 & 0.7 \\
0.6 & 0.6 & 1.0 & 0.6 & 0.5 & 0.8 & 0.6 & 0.6 & 0.8 & 0.5 & 0.6 & 1.0 & 0.6 & 0.6 \\
0.7 & 1.0 & 0.6 & 0.7 & 0.6 & 0.6 & 0.7 & 0.7 & 0.6 & 0.6 & 0.7 & 0.6 & 1.0 & 0.7 \\
1.0 & 0.7 & 0.6 & 0.7 & 0.6 & 0.6 & 0.7 & 0.7 & 0.6 & 0.6 & 0.7 & 0.6 & 0.7 & 1.0
\end{array}
\qquad (28)
$$

The column d concerns the time evolution of a wave packet initially at the centre d. In that column, the number at line j gives a majorant for the overlap of this time-dependent wave packet with a fictitious time-independent wave packet which would remains at centre j for

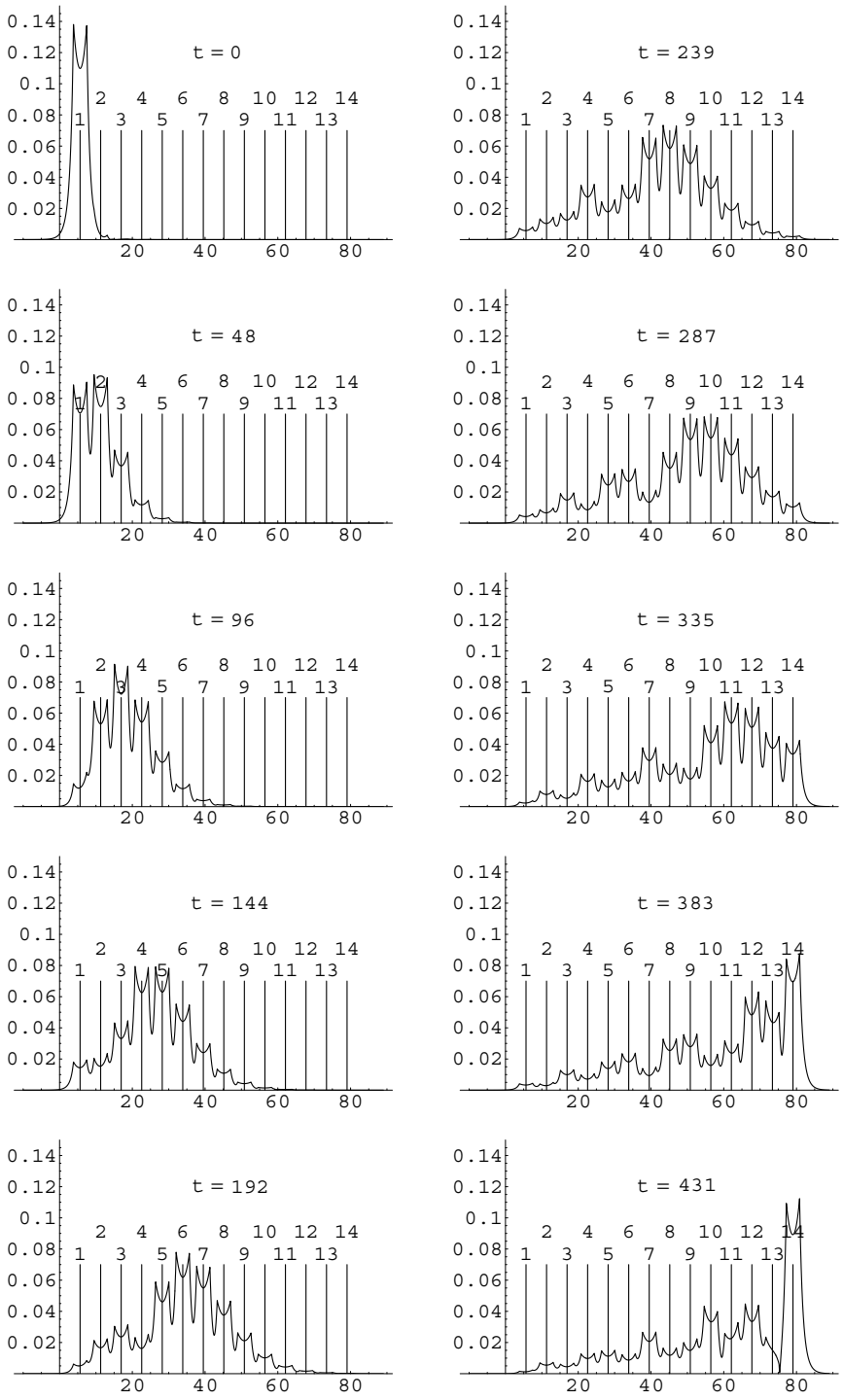

Figure 1. Abscissa: chain axis x. Ordinate: $|\langle x, y = 0, z = 0|\psi\rangle|$, the modulus of the normalized wavefunction on the chain axis. The intersections of the numbered vertical lines with the abscissa indicate the centres $\mathbf{a}_j$.

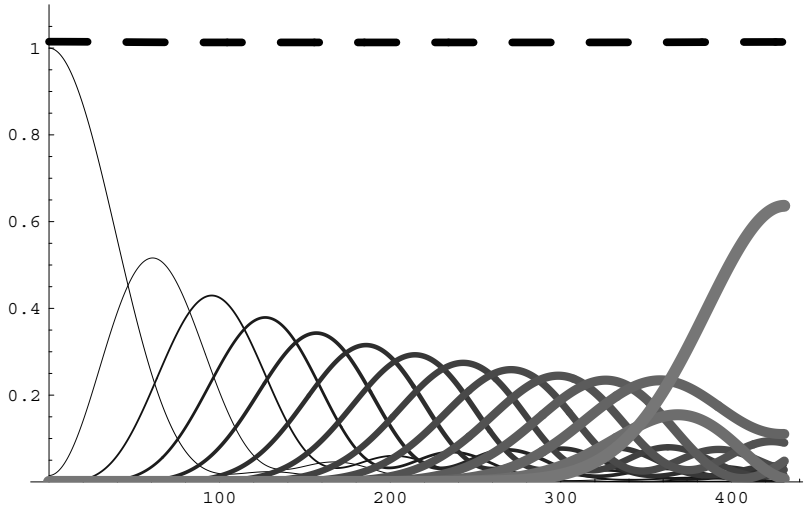

Figure 2. Abscissa: time t. Fourteen full line curves: $P_{j,1}(t)$ (see equation 26), $1 \leqslant j \leqslant 14$, with thickness and grey level increasing with j. The thick dashed line curve corresponding to $\sum_{j=1}^{14} P_{j,1}(t)$ remains in the vicinity of unity.

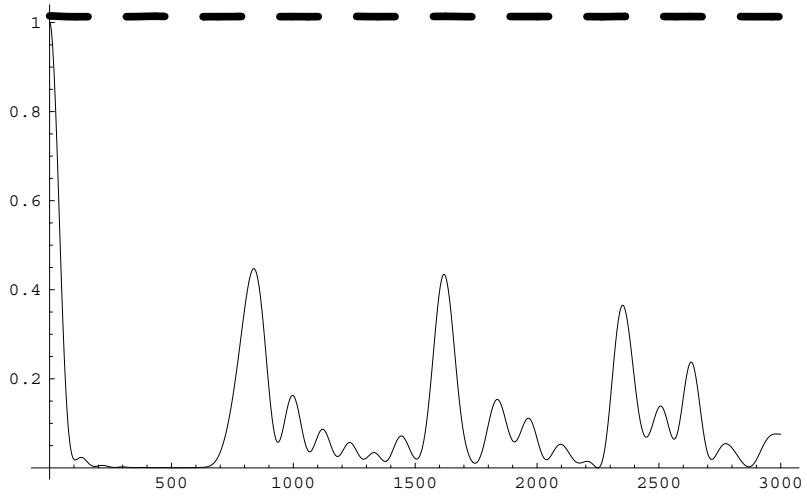

Figure 3. Abscissa: time t. Full line curves: $P_{1,1}(t)$ (see equation (26)). The thick dashed line curve corresponding to $\sum_{j=1}^{14} P_{j,1}(t)$ remains in the vicinity of unity.

all times. For example, $M_{3,1}$, the element at line 3 and column 1, is equal to 0.6 and this means that for a wave packet initially at the centre 1, the overlap $P_{3,1}(t)$ will remain smaller than or equal to 0.6 for all time values. The symmetry with respect to the second diagonal reflects the symmetry of the chain with respect to its middle. The interest in this matrix will come from the comparison with the analogue matrix for a Fibonacci chain and a Penrose structure in subsections 5.3, 5.4.

5.2. Truncated periodic linear chain with a defect

We consider the previous chain of subsection 5.1, and multiply the interval between centres 7 and 8 (see figure 1) by $7/5$. This is the only change. One has $R \simeq 1.03$. Figure 4 is the exact

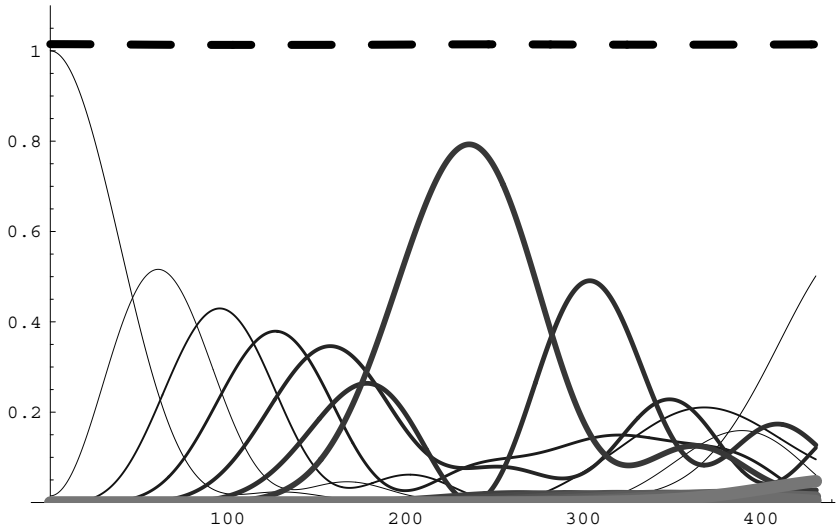

Figure 4. As figure 2, but for a chain with an interval between the centres 7 and 8 multiplied by 7/5. See text.

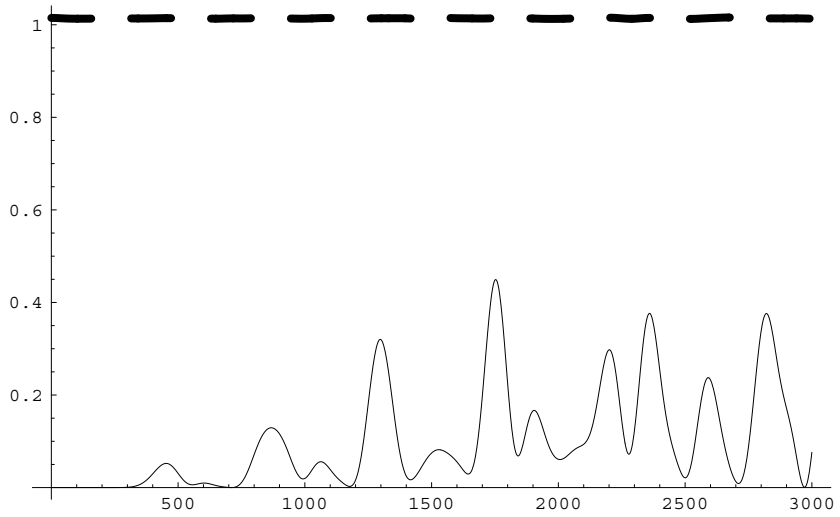

Figure 5. Chain with an interval between centres 7 and 8 equal to $7d/5$. See text. Abscissa: time t. Full line curves: $P_{1,14}(t)$ (see equation (26)). The thick line curve corresponding to $\sum_{j=1}^{14} P_{j,1}(t)$ remains in the vicinity of unity.

analogue of figure 2. It is seen that, over the same time interval, the coefficients $P_{j,1}(t)$ remain negligible for $j \geqslant 8$. The wave packet is thus reflected near centre $\mathbf{a}_7$ and the coefficient $P_{7,1}(t)$ presents a maximum approximately equal to 0.8. The first revival of the coefficient $P_{1,1}(t)$ becomes appreciable at the end of the time interval (the right extremity of figure 4). After sufficiently long times, however, the wave packet takes significant values inside the right second half part of the chain, as shown in figure 5, where the last coefficient $P_{14,1}(t)$ is plotted up to time 3000, together with the sum $\sum_{j=1}^{14} P_{j,1}(t)$.

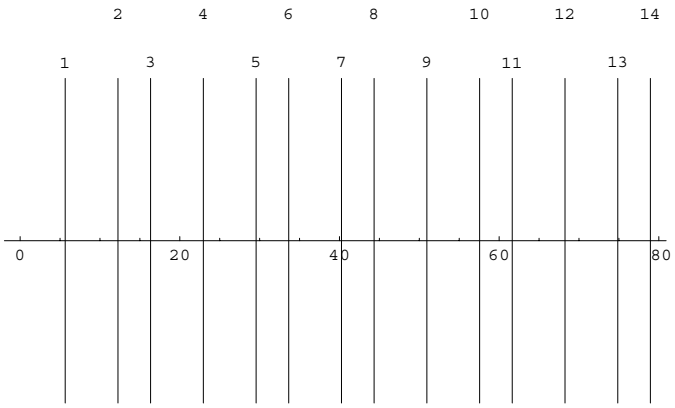

Figure 6. The 14 centres of the truncated Fibonacci chain are at the intersection of the vertical lines with the abscissa.

We finally consider the previous chain of subsection 5.1, and multiply the interval between centres 7 and 8 (see figure 1) by 3/5. This is the only change. One has $R \simeq 1.05$. The difference now is that the coefficient $P_{7,1}(t)$ remains negligible, the wave packet being reflected near centre $\mathbf{a}_6$. As a result, the reflection takes place slightly before the one in figure 4. The first revival of the coefficient $P_{1,1}(t)$ also takes place before the one of figure 4. The upper bounds $M_{7,1}$ and $M_{8,1}$ have small values, about 0.0168. Moreover, all the upper bounds $M_{j\notin\{7,8\},7}$ and $M_{j\notin\{7,8\},8}$ pertaining to an initial wave packet position at centres 7 and 8 respectively also remain smaller than 0.0715, whereas $M_{7,7}$, $M_{8,7}$, $M_{7,8}$, $M_{8,8}$ are equal to unity. The interpretation is clear: if the starting position of the wave packet is at centres 7 or 8, the wave packet oscillates between these two neighbouring centres, forming a (non-stationary) quasi-bounded state near the two centres. On the other hand, it is found that, over the same time interval, the coefficients $P_{j,1}(t)$ remain negligible for $j \geqslant 7$. As noted previously, the wave packet is thus reflected near the centre $\mathbf{a}_6$ and the coefficient $P_{6,1}(t)$ presents a maximum slightly greater than 0.8. After sufficiently long times, however, the wave packet takes significant values inside the right second half part of the chain.

It is natural that the reflection takes place near the centre 7 when the distance between centres 7 and 8 is expanded, but why does the reflection take place near centre 6 when the distance between centres 7 and 8 is reduced? The reason is that the ground state wavefunction, i.e. the eigenfunction of the Hamiltonian associated with the lowest energy eigenvalue, is then mainly concentrated near the two less distant centres 7 and 8. As a result of orthogonality of eigenfunctions associated with different energy eigenvalues, the initial wave packet has a small coefficient $\langle\psi_u|\chi_1\rangle$ (see equation (22)) with $|\psi_u\rangle$ denoting the ground state.

5.3. Truncated Fibonacci chain

The two intercentre distances have been chosen so as the number of centres per unit length is the same as for the previous truncated periodic linear chain in the limit of infinite number of centres. More specifically the large intercentre distance is $d_{jk} = 6.5183\frac{\sqrt{3}}{2}\tau\frac{\tau+1}{\tau+2} \simeq 6.6093$ au, and the short intercentre distance is $d_{jk} = 6.5183\frac{\sqrt{3}}{2}\frac{\tau+1}{\tau+2} \simeq 4.0848$ au, where τ denotes the golden ratio: $\tau = (1+\sqrt{5})/2$. Again, these are the values used in [18]. The number of centres is $N = 14$ as for the previous case in the truncated periodic linear chain, and the centres are at the intersections of vertical lines with the abscissa axis in figure 6. One has $R \simeq 1.07$.

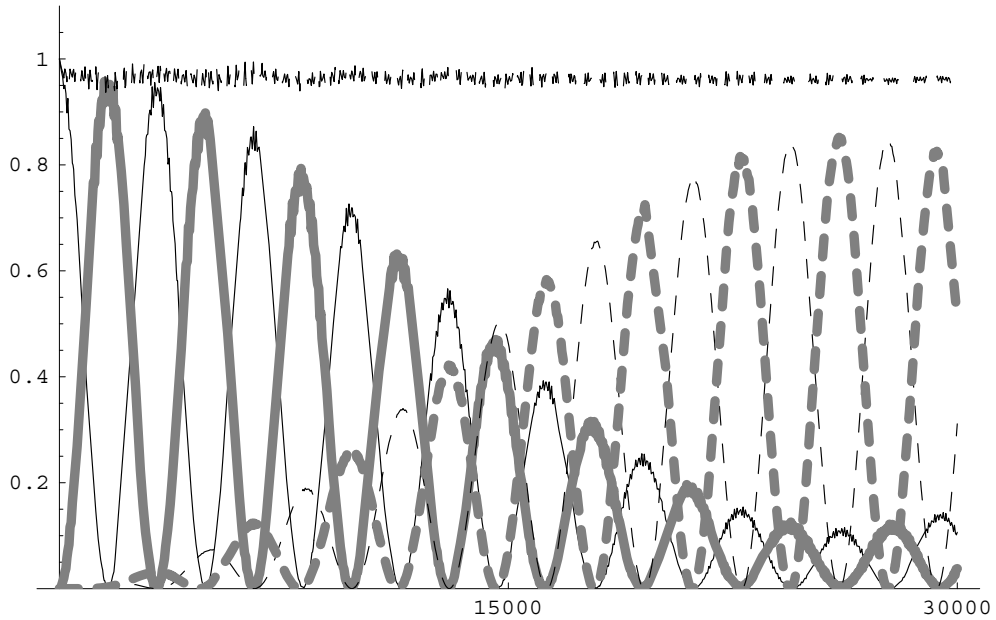

Figure 7. Abscissa: time t. Full line curve starting at unity: $P_{1,1}(t)$. Full thick line curve in phase opposition with the curve $P_{1,1}(t)$: $P_{4,1}(t)$. Dashed line curve starting at zero: $P_{9,1}(t)$. Thick dashed line curve in phase opposition with $P_{9,1}(t)$: $P_{12,1}(t)$. Dashed line curve remaining in the vicinity of unity: the sum over the previous four curves.

The majorant matrix M (each round to the first non-zero digits)

1.0	0.05	0.05	1.0	0.002	0.02	0.02	0.003	0.9	0.02	0.02	0.9	0.003	0.02
0.05	1.0	1.0	0.06	0.02	0.03	0.06	0.05	0.02	0.08	0.08	0.02	0.05	0.05
0.05	1.0	1.0	0.06	0.02	0.03	0.05	0.05	0.02	0.08	0.08	0.02	0.05	0.05
1.0	0.06	0.06	1.0	0.02	0.05	0.05	0.02	0.9	0.02	0.02	0.8	0.003	0.02
0.002	0.02	0.02	0.02	1.0	1.0	1.0	1.0	0.02	0.05	0.05	0.003	0.01	0.01
0.02	0.03	0.03	0.05	1.0	1.0	1.0	1.0	0.05	0.06	0.06	0.02	0.01	0.02
0.02	0.06	0.05	0.05	1.0	1.0	1.0	1.0	0.05	0.02	0.02	0.02	0.001	0.002
0.003	0.05	0.05	0.02	1.0	1.0	1.0	1.0	0.02	0.02	0.02	0.002	0.002	0.002
0.9	0.02	0.02	0.9	0.02	0.05	0.05	0.02	1.0	0.06	0.06	1.0	0.02	0.05
0.02	0.08	0.08	0.02	0.05	0.06	0.02	0.02	0.06	1.0	1.0	0.07	0.8	0.8
0.02	0.08	0.08	0.02	0.05	0.06	0.02	0.02	0.06	1.0	1.0	0.07	0.8	0.8
0.9	0.02	0.02	0.8	0.003	0.02	0.02	0.002	1.0	0.07	0.07	1.0	0.02	0.05
0.003	0.05	0.05	0.003	0.01	0.01	0.001	0.002	0.02	0.8	0.8	0.02	1.0	1.0
0.02	0.05	0.05	0.02	0.01	0.02	0.002	0.002	0.05	0.8	0.8	0.05	1.0	1.0

(29)

is in sharp contrast with the ones relative to the periodic case (equation (28)). The situation is thus quite different. Let us consider for example the majorants $M_{j,1}$, i.e. the first column for a wave packet initially at the centre 1. It is seen from the first column of upper bounds that the overlap coefficients $P_{j,1}(t)$ are negligible, except for centres 1, 4, 9, 12. The interpretation is easy if one looks at figure 6: the wave packet can take significant values only at the centres which do not have a closest neighbour at a short intercentre distance, that is to say at centres with the same surroundings. Figure 7 shows that the wave packet indeed takes significant values at these four centres, and it has to be noted that the transport is much slower than for

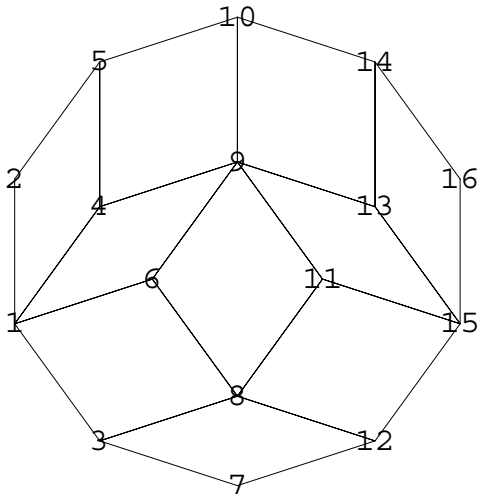

Figure 8. Truncated Penrose tiling with 16 centres.

the periodic case (the interval of times in figure 7 is $0 \leqslant t \leqslant 30\,000$). The very rapid small oscillations in the curves of figure 7 are due to the small coupling with the ten other centres.

If we now look at the second column of the majorant matrix, equation (29), we see that a wave packet starting at centre 2 will oscillate between this centre and the neighbouring centre 3, and will remain confined with essentially no spreading over the other centres.

The time evolution for a wave packet initially at centre 5 can also be predicted from the fifth column of matrix (29): it can take significant values only at centres 5, 6, 7, 8. It is also clear from this matrix that a wave packet initially at centre 11 can take significant values only at centres 10, 11, 13, 14.

The facts described in the last two paragraphs can be understood from knowledge of the stationary wavefunctions, i.e. eigenfunctions of the Hamiltonian. Some graphs of these wavefunctions can be found in figure 6(*b*) of [18]. These eigenfunctions are site selective, which means in particular that a wavefunction with significant values at a centre with a neighbour at short distance will not take significant values at a centre with left and right neighbours both at large distance and vice versa. This explains for example why a wave packet initially at centre 11 can take significant values only at centres 10, 11, 13, 14 but not at centre 12. Now the ground state wavefunction is mainly concentrated in the closest two short intervals, i.e. between centres 5 and 6, and between centres 7 and 8. Due to orthogonality between eigenstates of different energy, a wave packet initially at centre 2 has a small coefficient $\langle\psi_u|\chi_2\rangle$ (see equation 22) with $|\psi_u\rangle$ denoting the ground state, and therefore will oscillate between centres 2 and 3.

5.4. Truncated Penrose structure

A truncated Penrose tiling with 16 centres is reported in figure 8. The edges of rhombi are plotted for a better visualization, but only the vertex positions are relevant. This configuration is symmetric relative to a vertical axis through vertices 7, 8, 9, 10. The common edge length of the two rhombi is 6.0816 au, as in [17, 20]. One has $R \simeq 1.111\,39$. A systematic

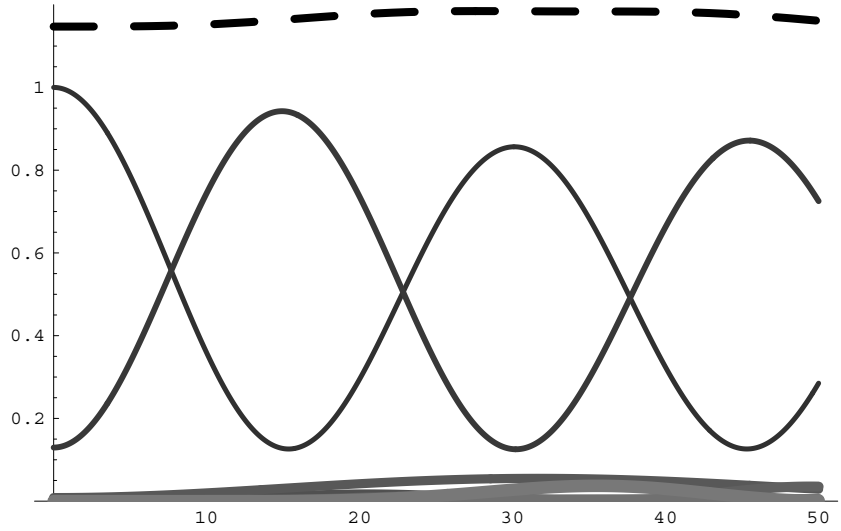

Figure 9. Truncated Penrose tiling with 16 centres. Abscissa: time t. Sixteen full line curves: $P_{j,7}(t)$ (see equation (26)), $1 \leqslant j \leqslant 16$, with thickness and grey level increasing with j. In particular, the full line starting at unity is $P_{7,7}(t)$, and in phase opposition is $P_{8,7}(t)$. The thick dashed line curve remaining in the vicinity of 1.15 : $\sum_{j=1}^{16} P_{j,7}(t)$.

study of time evolution of wave packets on a Penrose structure is beyond the scope of the present work. We only give the majorant matrix for the truncated Penrose tiling of figure 8.

1.0	0.3	0.9	0.06	0.4	0.3	0.01	0.01	0.08	0.1	0.3	0.9	0.06	0.4	1.0	0.3
0.3	1.0	0.2	0.6	0.4	1.0	0.06	0.06	0.2	0.05	1.0	0.2	0.6	0.4	0.3	1.0
0.9	0.2	1.0	0.02	0.3	0.2	0.07	0.06	0.03	0.09	0.2	1.0	0.02	0.3	0.9	0.2
0.06	0.6	0.02	1.0	0.04	0.6	0.05	0.06	0.02	0.004	0.6	0.02	1.0	0.04	0.06	0.6
0.4	0.4	0.3	0.04	1.0	0.4	0.007	0.006	0.2	0.4	0.4	0.3	0.04	1.0	0.4	0.4
0.3	1.0	0.2	0.6	0.4	1.0	0.03	0.03	0.3	0.05	1.0	0.2	0.6	0.4	0.3	1.0
0.01	0.06	0.07	0.05	0.007	0.03	1.0	1.0	0.03	0.009	0.03	0.07	0.05	0.007	0.01	0.06
0.01	0.06	0.06	0.06	0.006	0.03	1.0	1.0	0.02	0.007	0.03	0.06	0.06	0.006	0.01	0.06
0.08	0.2	0.03	0.02	0.2	0.3	0.03	0.02	1.0	0.4	0.3	0.03	0.02	0.2	0.08	0.2
0.1	0.05	0.09	0.004	0.4	0.05	0.009	0.007	0.4	1.0	0.05	0.09	0.004	0.4	0.1	0.05
0.3	1.0	0.2	0.6	0.4	1.0	0.03	0.03	0.3	0.05	1.0	0.2	0.6	0.4	0.3	1.0
0.9	0.2	1.0	0.02	0.3	0.2	0.07	0.06	0.03	0.09	0.2	1.0	0.02	0.3	0.9	0.2
0.06	0.6	0.02	1.0	0.04	0.6	0.05	0.06	0.02	0.004	0.6	0.02	1.0	0.04	0.06	0.6
0.4	0.4	0.3	0.04	1.0	0.4	0.007	0.006	0.2	0.4	0.4	0.3	0.04	1.0	0.4	0.4
1.0	0.3	0.9	0.06	0.4	0.3	0.01	0.01	0.08	0.1	0.3	0.9	0.06	0.4	1.0	0.3
0.3	1.0	0.2	0.6	0.4	1.0	0.06	0.06	0.2	0.05	1.0	0.2	0.6	0.4	0.3	1.0

(30)

As can be seen from this matrix and from figure 8, the time evolution is clearly site selective. Consider for example a wave packet initially at centre 7 (column 7). The seventh column of the above matrix tells us that the wave packet will remain confined between centres 7 and 8. The oscillations between these centres are rapid as shown in figure 9, where the time interval is $0 \leqslant t \leqslant 50$. It should be noted that initially, $P_{8,7}(0)$ has a value of about 0.15. Consider then a wave packet initially at centre 4. The fourth column of matrix (30) tells us that the wave packet can take significant values only at centres 2, 4, 6, 11, 13, 16, i.e. at the centres located on two adjacent short diagonals of thin rhombi.

6. Concluding remarks

The present work first provides a model for the general study of time evolution of wave packets bound in nanosystems of arbitrary geometry in three-dimensional space with little numerical effort. For each geometric configuration, the eigenvalues of the Hamiltonian have to be computed accurately since precise eigenvalues are necessary for accurate eigenvector determination. The difference between neighbouring eigenvalues is also important for time evolution, and these differences can be quite small in cases of quasicrystals whose spectra are of fractal nature. Secondly, the present work provides for this model methods and tools for analysing wave packet time evolution. These methods and tools are particularly suitable for a systematic study of the influence of the starting position of the wave packet.

The phenomena described in this paper may be physically relevant to experiments involving scanning tunnelling microscopy, or ultrashort laser pulses. They may be of interest for nanosystems on a surface or for macromolecules. In any case, even if not directly accessible to experiments by present day technology, they should be born in mind for theoretical descriptions of transport phenomena.

The interpretation of many non-intuitive effects has been made in terms of eigenfunctions of the Hamiltonian in subsections 5.2 and 5.3. The key point is that orthogonality between eigenfunctions pertaining to different energy eigenvalues is achieved differently in (truncated) periodic systems and in (truncated) quasiperiodic systems. In truncated periodic systems, each eigenfunction covers the whole range of the system, and orthogonality is achieved by oscillations. In truncated quasiperiodic systems, the eigenfunctions are site selective [18, 20] and some may be confined. (No confinement for *infinite* quasiperiodic systems.) Orthogonality may then be achieved not only by oscillations, but also simply by main localization in different regions. Once the stationary wavefunctions have been computed for a particular geometric configuration of the system, it is rather easy to explain *a posteriori* the overall aspect of these functions, starting from the one of lowest energy. It is however not always easy to make predictions before doing computations. Hence the interest in a solvable model.

Appendix A. Computation of a matrix element

Following the method described in the appendix of [18], one first obtains

$$\langle \xi_j | G_0(z_2) G_0(z_1) | \xi_k \rangle = (2m)^2 \frac{r}{d_{jk}} \frac{1}{\pi} \int_{-\infty}^{\infty} \mathrm{d}p \frac{\sin^2(pr)}{(p^2 - p_2^2)(p^2 - p_1^2)} \frac{\sin(pd_{jk})}{p}$$

For the case $d_{jk} > 2r$, one proceeds as in the appendix of [18] by expressing $\sin(pd_{jk})$ as the sum of two exponentials and closing the contour by an infinite semi-circle in the upper half plane for the term $\exp(\mathrm{i}pd_{jk})$ and in the lower half plane for the term $\exp(-\mathrm{i}pd_{jk})$.

The case $d_{jk} < 2r$ is slightly more complicated. One first expands the square sine in terms of exponentials:

$$\langle \xi_j | G_0(z_2) G_0(z_1) | \xi_k \rangle = -2m^2 \frac{r}{d_{jk}} \frac{1}{2\pi} \int_{-\infty}^{\infty} \mathrm{d}p \frac{1}{(p^2 - p_2^2)(p^2 - p_1^2)} [\exp(\mathrm{i}2pr) + \exp(-\mathrm{i}2pr) - 2] \frac{\sin(pd_{jk})}{p}.$$

The term involving $\exp(\mathrm{i}2pr)\frac{\sin(pd_{jk})}{p}$ can be evaluated by closing the contour by an infinite semi-circle in the upper half plane. The term involving $\exp(-\mathrm{i}2pr)\frac{\sin(pd_{jk})}{p}$ can be evaluated by closing the contour by an infinite semi-circle in the lower half plane. There remains the

term involving $-2\frac{\sin(pd_{jk})}{p}$. This quotient is regular at $p = 0$, but when expressing $\sin(pd_{jk})$ as the sum of two exponentials, we obtained two terms singular at $p = 0$. A well-known method consists in an infinitesimal modification of the contour in order to avoid the point $p = 0$ slightly below or above. This does not change the result since $\frac{\sin(pd_{jk})}{p}$ is continuous at $p = 0$. Application of the residue theorem finally leads to equation (13).

References

[1] Dittrich T, Hänggi P, Ingold G L, Kramer B, Schön G and Zwerger W 1998 *Quantum Transport and Dissipation* (New York: Wiley)

[2] Liboff R L 2003 *Kinetic Theory, Classical, Quantum, and Relativistic Descriptions (Graduate Texts in Contemporary Physics)* 3rd edn (New York: Springer)

[3] Yeazell J A and Uzer T 2000 *The Physics and Chemistry of Wave Packets* (New York: Wiley)

[4] Meinhold D, Rosam B, Löser F, Lyssenko V G, Rossi F, Zhang Jian-Zhong, Köhler K and Leo K 2002 *Phys. Rev.* B **65** 113302

[5] Triozon F, Vidal J, Mosseri R and Mayou D 2002 *Phys. Rev.* B **65** 220202(R)

[6] Simanjuntak H P and Pereyra P 2003 *Phys. Rev.* B **67** 045301

[7] Konsek S L and Pearsall T P 2003 *Phys. Rev.* B **67** 045306

[8] Zozoulenko I V and Blomquist T 2003 *Phys. Rev.* B **67** 085320

[9] Vidal J, Destainville N and Mosseri R 2003 *Phys. Rev.* B **68** 172202

[10] Yuan H Q, Grimm U, Repetowicz P and Schreiber M 2000 *Phys. Rev.* B **62** 15569

[11] Rotter S, Tang J Z, Wirtz L, Trost J and Burgdörfer J 2000 *Phys. Rev.* B **62** 1950

[12] Márk G I, Biró L P, Gyulai J, Thiry P A, Lucas A A and Lambin P 2000 *Phys. Rev.* B **62** 2797

[13] Aronstein D L and Stroud C R Jr 2000 *Phys. Rev.* A **62** 022102

[14] Vugalter G A, Das A K and Sorokin V A 2002 *Phys. Rev.* A **66** 012104

[15] Robinett R W and Heppelmann S 2002 *Phys. Rev.* A **65** 062103

[16] Gaeta Z D, Noel M W and Stroud C R Jr 1994 *Phys. Rev. Lett.* **73** 636

[17] de Prunelé E 1997 *J. Phys. A: Math. Gen.* **30** 7831

[18] de Prunelé E and Bouju X 2001 *Phys. Status Solidi* b **225** 95

[19] Bouju X and de Prunelé E 2000 *Phys. Status Solidi* b **217** 819

[20] de Prunelé E 2002 *Phys. Rev.* B **66** 094202

[21] de Prunelé E 2003 *J. Phys. A: Math. Gen.* **36** 8797